Accepted Manuscript

Multiaxial cyclic behaviour and fatigue modelling of AM30 Mg alloy extrusion

Ali A. Roostaei, Hamid Jahed

PII: S0142-1123(16)30453-4
DOI: http://dx.doi.org/10.1016/j.ijfatigue.2016.12.037
Reference: JIJF 4188

To appear in: *International Journal of Fatigue*

Received Date: 9 September 2016
Revised Date: 1 December 2016
Accepted Date: 27 December 2016

Please cite this article as: Roostaei, A.A., Jahed, H., Multiaxial cyclic behaviour and fatigue modelling of AM30 Mg alloy extrusion, *International Journal of Fatigue* (2016), doi: http://dx.doi.org/10.1016/j.ijfatigue.2016.12.037

Multiaxial cyclic behaviour and fatigue modelling of AM30 Mg alloy extrusion

Ali A. Roostaei, Hamid Jahed *

Mechanical and Mechatronics Engineering Department, University of Waterloo, 200 University Ave. W. Waterloo, ON, Canada N2L 3G1

Abstract

Multiaxial fatigue characteristics of AM30 Mg alloy extrusion are studied through fully-reversed strain-controlled cyclic experiments including pure torsional and combined axial-torsional at 0, 45 and 90° phase angle shifts. Under pure torsional cyclic loading, AM30 extrusion is realized to exhibit better fatigue properties than AZ31B and AZ61A extrusions, especially in low-cycle fatigue regime. Under proportional axial-torsional cyclic loading, twinning/de-twinning in axial mode results in asymmetric shear hysteresis loop. The effect of non-proportionality of biaxial loading on various aspects of material response is also examined and observed to be depending on the magnitude of axial strain amplitude. Finally, the life prediction capabilities of two critical plane models, i.e., modified Smith-Watson-Topper (SWT) and Fatemi-Socie (FS), as well as Jahed-Varvani (JV) energy-based approach are assessed, employing fatigue life data of AM30 extrusion. Correlation data between experimental and estimated lives are found to lie within narrow scatter band.

Keywords: Magnesium alloys; Multiaxial fatigue; Cyclic properties; Fatigue modelling; Strain energy density.

1. Introduction

Saving energy and conservation of environment are two major reasons for drawing automotive industries' attention to wrought magnesium alloys as a light structural metal [1,2]. It

* Corresponding author;
Email addresses: aaroostaei@uwaterloo.ca (A.A. Roostaei), hjahed@uwaterloo.ca (H. Jahed).

was stated that diminishing the vehicle's weight by 10% would bring about a saving of approximately 5% in fuel consumption, assuming the appropriate adjustment of engine and gearbox performance [3].

Magnesium alloys are, currently, being utilized for making non-load bearing components, e.g., housing and trim parts [3,4]. To exploit their full weight-saving potential, their application needs to be broadened to load bearing components, such as body and suspension parts. Under vehicle's normal service conditions, these parts, are subjected to cyclic loading in multiaxial stress state, and thereby, prone to fatigue failure. Although the load bearing parts are generally designed to operate under low cyclic stresses in high cycle fatigue regime, they may locally experience high cyclic stresses at notches and other geometrical complexities. In light of what has been said above, understanding the multiaxial fatigue response of magnesium alloys is imperative to ensure the reliability and safety of vehicles throughout their service life.

Twenty years ago, Bentachfine et al. [5] performed strain-controlled axial-torsional tests on a magnesium-lithium alloy extrusion at various phase angle shifts in the range of 0 to 180°. They concluded that increasing phase angle shift from 0 to 90° decreases fatigue life, which was related to the generation of more complex defect structure and higher dislocation density as results of constant rotation of principal strain axes with respect to grain orientation. Since that time, there were only a few studies dealing with the multiaxial deformation and fatigue of wrought magnesium alloys. Yu et al. [6] conducted fully-reversed strain-controlled pure axial, pure torsional and combined axial-torsional cyclic tests on AZ61A extrusion. Employing an equivalent strain amplitude parameter defined as the radius of a circle circumscribing loading path, they reported the highest resistance to fatigue failure under proportional loading and the shortest fatigue life under 90° out-of-phase loading. It was, further, shown that Fatemi-Socie

(FS) and modified Smith-Watson-Topper (SWT) models were able to acceptably predict experimental fatigue life. In another study by the same authors (Zhang et al. [7]), cyclic deformation characteristics of AZ61A extrusion were explored. Slight cyclic hardening and insignificant non-proportional hardening were observed under various loading conditions. The asymmetry of shear hysteresis loop in combined axial-torsional tests was attributed to the successive occurrence of twinning/de-twinning under axial deformation mode. Similar to the work by Yu et al. [6], Xiong et al. [8] investigated AZ31B extrusion and reached to the same conclusion regarding fatigue resistance under different loading conditions. Moreover, they evaluated the modified SWT and Jiang critical plane models capable of predicting fatigue life under multiaxial loading conditions. Albinmousa et al. [9–12] carried out fully-reversed strain-controlled cyclic tests, including pure axial, pure torsional, and combined axial-torsional proportional and non-proportional at 45 and 90° phase angle shifts, on AZ31B extrusion. Their results demonstrated that AZ31B extrusion exhibited additional hardening because of non-proportionality, but not due to multiaxiality. Notwithstanding this non-proportional hardening, it was reported that phase angle shift had no significant influence on obtained fatigue life. In regard to fatigue modelling done by Albinmousa et al., Fatemi-Socie and Jahed-Varvani models resulted in better fatigue life estimations. Recently, Castro and Jiang [13] examined three critical plane approaches, i.e., SWT, FS and Jiang, using various uniaxial and multiaxial cyclic tests on AZ31B extrusion. It was deduced that FS and Jiang models gave reasonable fatigue life predictions and only Jiang model made a good correlation of cracking direction, which was ascribed to the mixed cracking mode of AZ31B extrusion. More recently, Li et al. [14] studied the multiaxial cyclic response of AZ31 extrusion during strain and stress-controlled experiments. From strain-controlled tests, they observed cyclic hardening in both axial and torsional

directions, as well as additional hardening due to multiaxiality in torsional mode. They also concluded that axial ratcheting during multiaxial stress-controlled tests depended on the shape of loading path in addition to the non-proportionality of loading. Circular 90° out-of-phase loading path generated the largest axial ratcheting strain.

The literature reviewed herein were all on the multiaxial study of AZ family of wrought magnesium alloys, especially AZ31B extrusion. To the best of authors' knowledge, no comprehensive study has thus far been done on the multiaxial behaviour of AM family of wrought Mg alloys, specifically AM30 extrusion. This article is, therefore, aimed at providing such study. Besides, in order to complement the uniaxial experimental cyclic data on AM30 extrusion presented by authors in [15], extensive pure torsional experiments have been conducted. The capabilities of two strain-based models, i.e., Fatemi-Socie and modified Smith-Watson-Topper, and an energy-based model, i.e., Jahed-Varvani, to predict fatigue life under general loading conditions are also investigated.

2. Material and methods

Experimental material for present study was hot-extruded AM30 magnesium alloy developed by Luo and Sachdev [16]. The details of the experimental alloy including its chemical composition and hot extrusion process parameters can be found in [17]. Thin-walled tubular specimens were machined from extrusion section along extrusion direction with the geometry and dimensions shown in Figure 1. It is worth noting that in order to make sure of microstructural uniformity, center region of the extrusion section (away from surface) were used for machining the specimens [18]. Figure 2 schematically shows the extrusion section and the location where the tubular specimens were cut from. The orientation of HCP crystals in

connection with defined section directions, i.e., extrusion (ED), transverse (TD) and normal (ND), is also depicted in Figure 2.

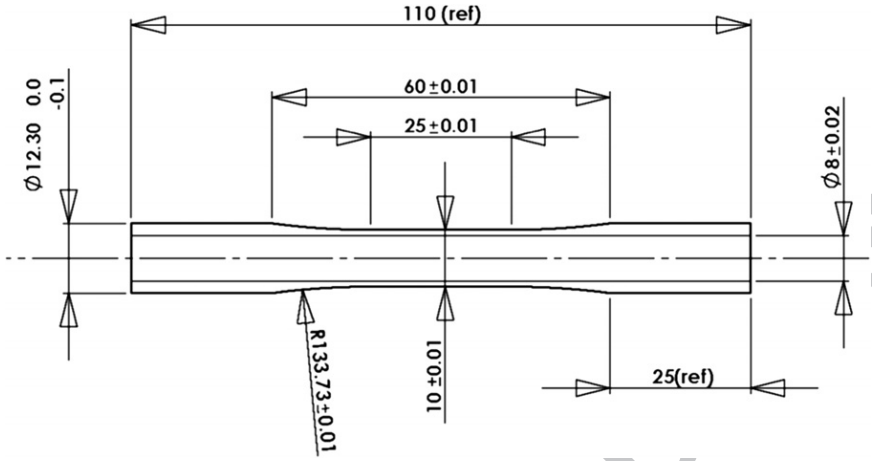

Figure 1. Tubular specimen geometry for pure torsional and biaxial tests.

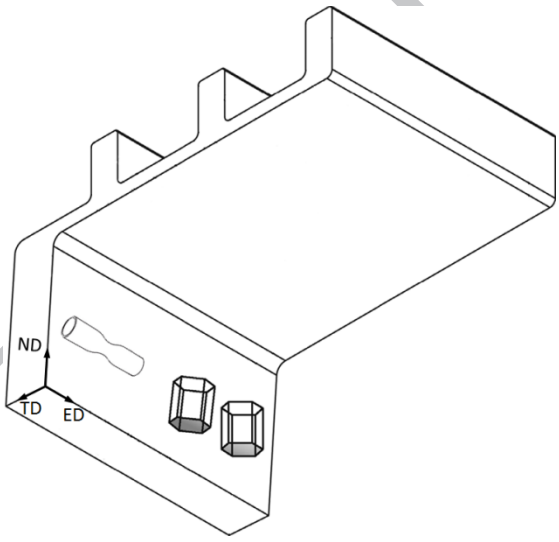

Figure 2. Schematic illustration of extrusion section showing crystal orientation in portion used for machining tubular specimens.

Fatigue experiments were conducted using an Instron 8874 servo-hydraulic biaxial machine with axial and torsional load capacities of ±25 kN and 100 N.m, respectively. All of the experiments were done under fully-reversed ($R_{\varepsilon\ or\ \gamma} = -1$) strain-controlled condition at ambient temperature. Axial tension-compression cyclic data along ED were taken from previous publication [15]. Epsilon biaxial extensometer (model 3550) with the axial and shear strain

ranges of ±5% and ±3°, mounted on specimen's gauge length, was employed to record engineering axial and shear strains. Sinusoidal waveforms with different phase angle shifts of 0, 45 and 90° were applied for proportional and non-proportional axial-torsional tests. Pure torsional tests were run at frequencies ranging from 0.03 to 0.4 Hz, depending on applied shear strain amplitude. At very low shear strain amplitudes, after material stabilized, tests were stopped to remove the extensometer. The tests were, then, resumed running at higher frequencies up to 8 Hz under torque-controlled condition. Axial-torsional tests were done at lower frequencies between 0.1 and 0.3 Hz. Failure criteria were assumed to be either final rupture of the specimen or 50% drop in maximum load, whichever came first, unless stated otherwise. The stress-strain curve at half-life was identified as stabilized stress-strain response.

Texture measurements were performed via a Bruker D8 Discover X-ray diffractometer equipped with a VÅNTEC-500 2D detector using Cu-K_α beam radiation at 40 kV and 40 mA.

3. Results and discussion

3.1. Pure torsional cyclic loading

3.1.1. Hysteresis loops

Stabilized shear stress-shear strain hysteresis loops of AM30 extrusion subjected to pure torsional loading are illustrated in Figure 3. Eleven shear strain amplitudes in the range of 0.4% to 2.5% are employed to fully characterise the torsional behaviour of the experimental alloy. Unlike its axial cyclic behaviour, explored elsewhere [15], AM30 extrusion possesses normal symmetric hysteresis loops under torsion. This can more clearly be seen from Figure 4, where the maximum and minimum tips of hysteresis loops at various shear strain amplitudes are plotted in one graph. From this figure, it can also be concluded that no significant mean stress is developed upon cyclic torsion testing. The observed symmetry alludes to the dominance of slip

deformation mechanisms, although the occurrence of twinning was also reported at high shear strain amplitudes [7,8,19]. The slightly sigmoidal shape of hysteresis loop at shear strain amplitude of 2.5% (can also be seen from Figure 7c) is probably due to twinning, which is in consistence with twin observation by other researchers.

To contrast monotonic with cyclic shear flow, monotonic shear stress-shear strain curve of AM30 extrusion up to 3% shear strain is also included in Figure 4. It is seen that stresses from cyclic curve are higher than the ones from monotonic curve. Cyclic shear hardening coefficient, K_s', and exponent, n_s', are calculated to be 335.6 MPa and 0.3023, respectively, while monotonic shear hardening coefficient, K_s, and exponent, n_s, are 154.78 MPa and 0.2019. The results suggest that AM30 extrusion shows greater hardening capacity when subjected to cyclic shear deformation. Hardening disparity between cyclic and monotonic data grows with the shear strain to reach to roughly 25% increase in shear stress at the shear strain of 2.5%.

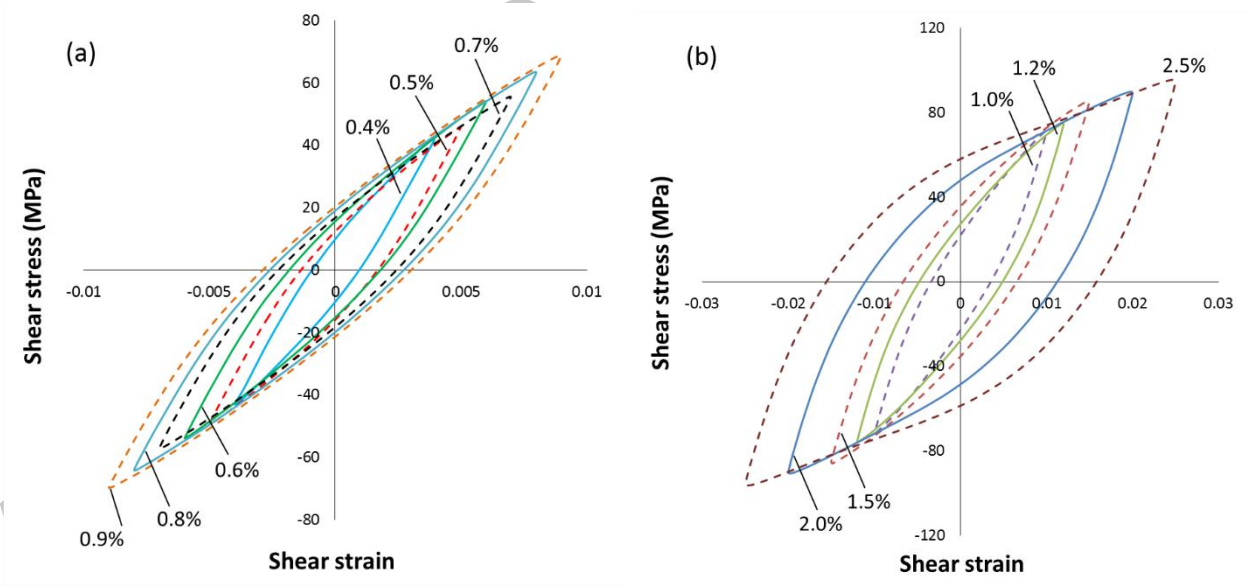

Figure 3. Half-life hysteresis loops of AM30 extrusion at different strain amplitudes under pure torsion.

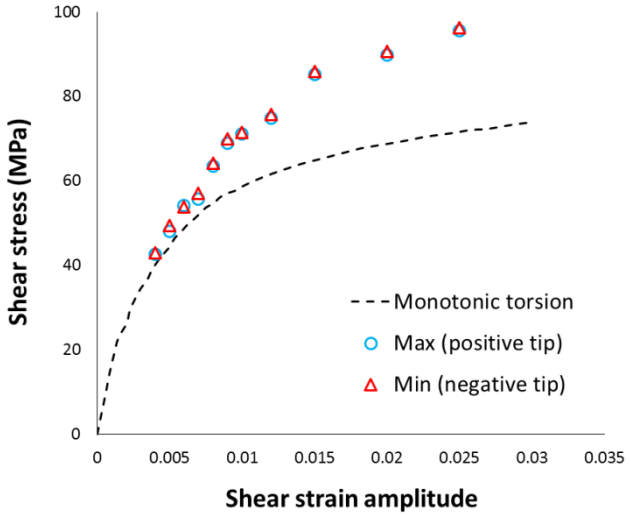

Figure 4. Cyclic and monotonic shear stress-shear strain curves of AM30 extrusion.

Texture measurements represented by basal (0002) and prismatic $(10\bar{1}0)$ pole figures can be used to verify twin occurrence at high shear strain amplitudes. Figure 5(a) shows pole figures of as-extruded material and Figure 5(b) shows pole figures of a specimen subjected to 2.5% cyclic shear strain amplitude. XRD measurements in Figure 5(b) were done on a section far away from final fatigue crack. According to Figure 5(a), the as-extruded material displays a rather strong basal texture with the majority of (0002) poles lying almost parallel to normal direction (ND), noting the peak intensity of 18.74 MUD (multiples of uniform distribution). The reduction of peak intensity of basal poles to 9.96 MUD and emergence of new texture components in Figure 5(b) can only be justified by the formation of mechanical twins during pure torsional straining. However, mechanical twinning does not seem to have a noticeable effect on the symmetry of shear hysteresis loops (Figure 3 and Figure 7). This probably hints at the equal amount of twinning/de-twinning under positive and negative shear stresses, because of the rotational symmetry of basal poles about extrusion direction [7].

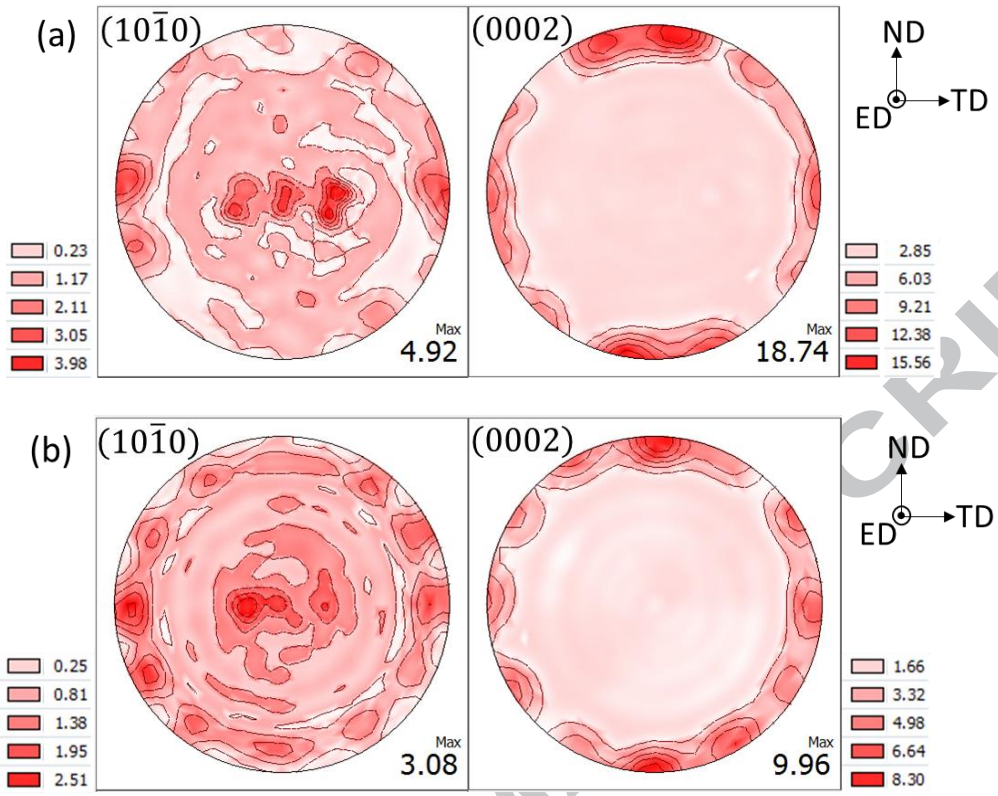

Figure 5. Basal and prismatic pole figures of (a) as-extruded material and (b) specimen tested under pure torsion at 2.5% shear strain amplitude.

The variations of shear stress amplitude with cycling at different shear strain amplitudes are depicted in Figure 6. As is seen, AM30 extrusion hardens during cyclic shear straining. However, the rate of hardening depends on the strain amplitude. Generally, the hardening rate increases with increasing shear strain amplitude. This increase in hardening rate is more pronounced for the shear strain amplitudes above 1%. This may be due to the occurrence of twinning at high shear strain amplitudes, which hinders free dislocation movements [7]. These results are in accordance with the cyclic shear behaviour reported for AZ61A extrusion [7]. Moreover, compared to AZ31B extrusion [12], the experimental alloy exhibits stronger cyclic shear hardening. The overall cyclic shear hardening response can also be inferred from Figure 7, where second-cycle along with the half-life hysteresis loops at low, intermediate and high shear strain amplitudes are plotted.

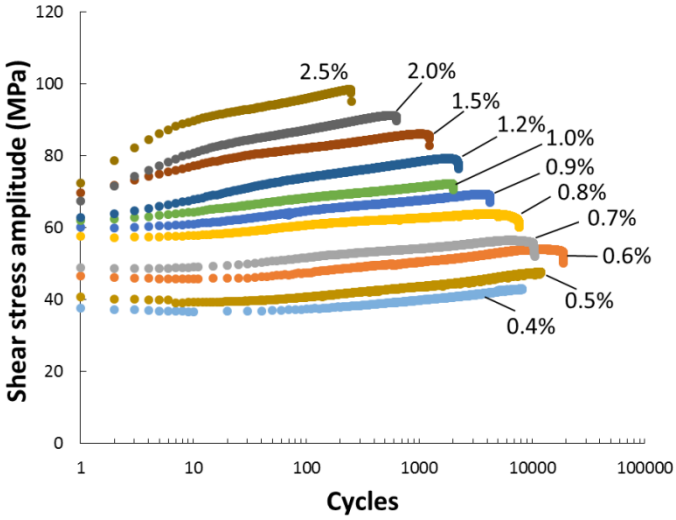

Figure 6. Shear stress amplitude evolution with cycling at various shear strain amplitudes.

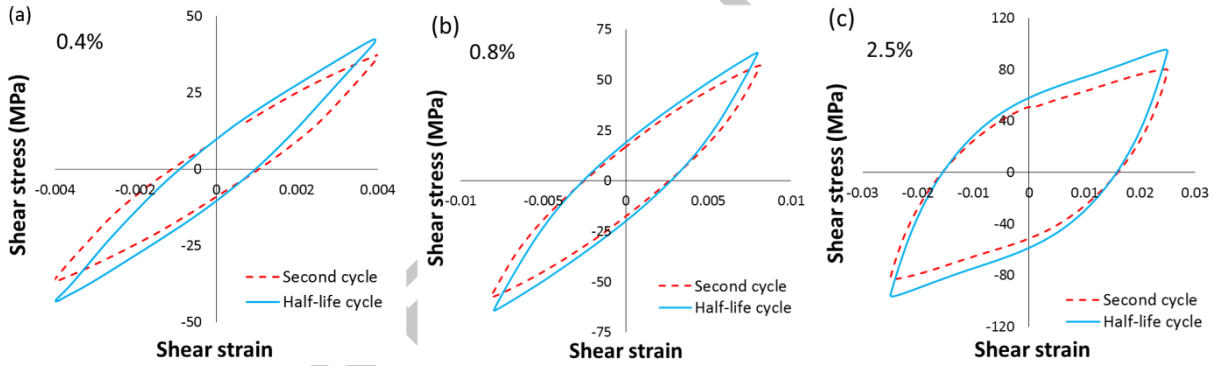

Figure 7. Typical shear hysteresis loops of AM30 extrusion at second and half-life cycles during cyclic tests at (a) low, (b) intermediate, and (c) high shear strain amplitudes.

3.1.2. Shear strain-life curve

Total shear strain amplitude as a function of number of cycles before fatigue failure for the experimental alloy under pure torsional loading is shown in Figure 8. For comparison purposes, shear strain-life data for AZ31B and AZ61A Mg alloy extrusions from literature [6,8] are also included. An arrow associated with a data point denotes a run-out test for which fatigue failure has not occurred at one million cycles. It should be mentioned here that the shear fatigue life data from this study are reported at 5% drop of maximum shear stress in a loading cycle, to

be consistent with the fatigue life data from literature. It is, however, observed that, in most cases, final failure happens either quickly or after a few cycles upon initial load drop. According to results from strain-controlled cyclic experiments displayed in Figure 8, AM30 extrusion shows better low-cycle shear fatigue properties than AZ31B and AZ61A extrusions. Considering the fact that at large strains, enhanced fatigue life depends more on ductility [20], the observed behaviour can be connected with the better formability of AM30 extrusion [16,18]. High-cycle shear fatigue properties of these alloys may be better contrasted by conducting stress-controlled cyclic tests.

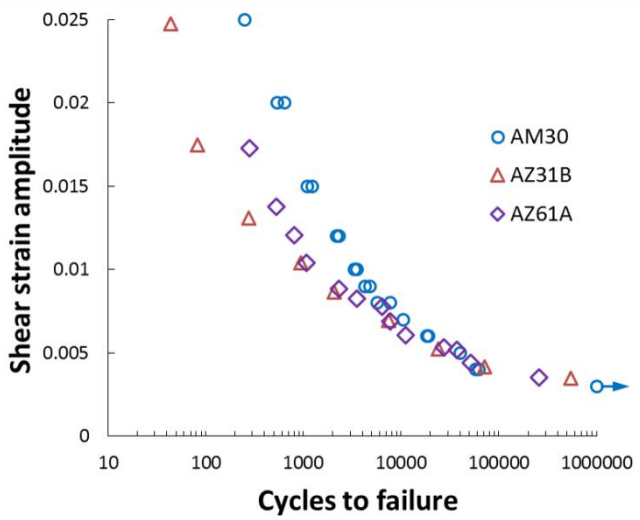

Figure 8. Shear strain-life data for AM30 extrusion compared with data for other wrought Mg alloys (AZ31B [8] and AZ61A [6]).

3.2. Combined axial-torsional cyclic loading

The details of the axial-torsional experiments including applied strain amplitudes, axial and shear stress ranges and mean values and experimental fatigue lives are tabulated in Table 1. The stress ranges and mean values are extracted from half-life (stabilized) hysteresis loops under axial and torsional deformation modes. It is also to be noted that the middle number of specimen ID denotes phase angle difference between axial and torsional deformation modes. In following sections, the axial-torsional cyclic behaviour of AM30 extrusion will be explored from two

perspectives: the interrelation of deformations in two different axes, and the influence of phase angle shift between axial and torsional loading cycles on cyclic hardening, hysteresis loops as well as obtained fatigue lives.

Table 1. Proportional and non-proportional combined axial-torsional fatigue tests' results.

Spec. ID	ε_a (%)	γ_a (%)	$\Delta\sigma$ (MPa)	σ_m (MPa)	$\Delta\tau$ (MPa)	τ_m (MPa)	N_f (cycles)
BA-0-3	0.3	0.4	235.7	11.8	79.3	1.4	8911
BA-0-10	0.3	0.4	225.2	11.5	78.5	2.1	9197
BA-0-2	0.4	0.4	310.9	46.1	72.9	6.2	1520
BA-0-7	0.4	0.4	300.1	41.7	72.6	4.9	1554
BA-0-4	0.5	0.4	355.2	55.6	68.3	6.7	1157
BA-0-8	0.5	0.6	330.2	42.9	87.4	6.2	917
BA-0-11	0.4	0.6	276.7	37.2	97.7	6.7	1629
BA-0-12	0.3	0.6	223.6	20.3	99.5	5.1	3210
BA-0-5	0.4	0.3	294.8	31.4	58.0	4.6	4027
BA-0-9	0.4	0.5	302.0	48.0	84.5	5.8	1495
BA-45-1	0.3	0.4	229.4	12.8	83.5	0.5	6085
BA-45-2	0.5	0.6	345.6	50.1	107.0	-2.7	650
BA-45-3	0.5	0.6	349.2	55.0	115.3	-3.4	669
BA-45-4	0.3	0.6	230.0	10.3	104.8	1.3	3141
BA-90-1	0.3	0.4	231.2	5.4	83.6	-2.3	6737
BA-90-2	0.5	0.6	347.4	39.5	123.1	-6.1	829
BA-90-3	0.3	0.4	237.7	0.9	87.0	-1.7	7508
BA-90-4	0.3	0.6	244.1	9.2	110.6	-2.9	3179

ε_a: Axial strain amplitude; γ_a: Shear strain amplitude; $\Delta\sigma$: Axial stress range; σ_m: Mean axial stress; $\Delta\tau$: Shear stress range; τ_m: Mean shear stress; N_f: Fatigue life.

3.2.1. Multiaxial deformation effects

The effect of simultaneous shear deformation on the shape of axial hysteresis loop and the evolution of axial stress amplitude during proportional (in-phase) axial-torsional tests are depicted in Figure 9. The proportional tests comprise axial strain amplitude of 0.5% and various shear strain amplitudes of 0, 0.4 and 0.6%. A closer look at Figure 9(a) reveals that the accompanied shear strain does not affect twinning/de-twinning-dominated portions of the axial hysteresis loops, at the end of compressive reversal and the initial stage of tensile reversal. However, the hardening rate of slip-dominated portion that follows de-twinning saturation is decreased with increasing accompanied shear strain. In other words, slip happens with less resistance in the co-presence of larger shear strain. This may be explained by the fact that accompanied shear stress will contribute to resolved shear stress on a specific slip plane to reach to its critical value (CRSS), and thereby, accommodate axial strain under lower axial stress.

It is known that axial cyclic hardening of AM30 extrusion can be related to the formation of residual twins due to successive twinning/de-twinning processes in each cycle [18,21]. On one hand, twinned area is rotated towards plastically hard orientations [22]. On the other hand, the residual twins' boundaries hinder dislocation motions on active slip planes [23]. However, as is seen from Figure 9(b), the hardening effect of residual twins is found to be attenuated, presumably through larger driving force provided by concomitant shear deformation, which can help dislocation advancement.

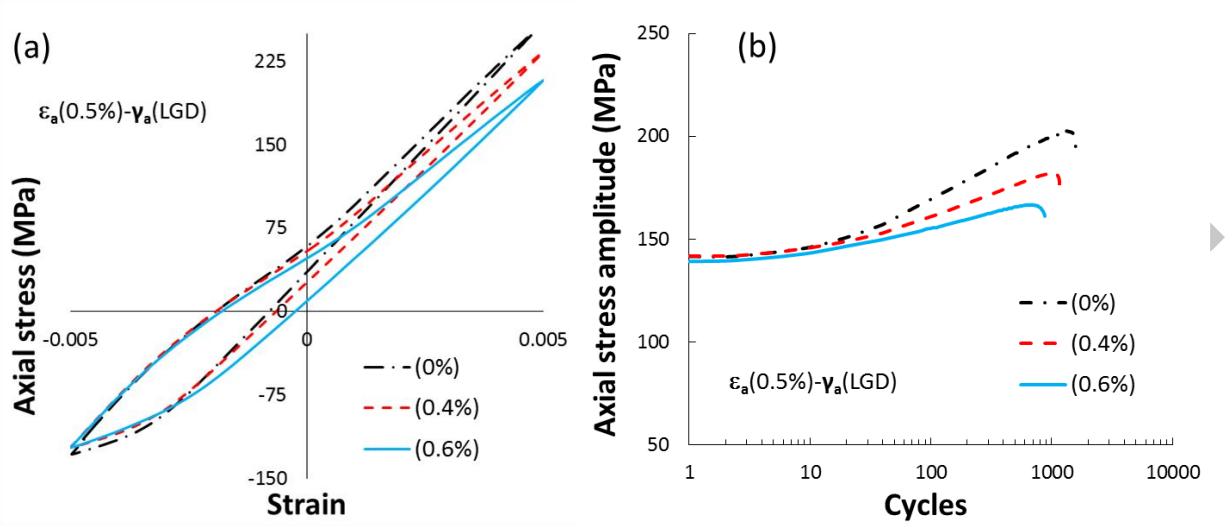

Figure 9. (a) Axial stress-strain hysteresis loops and (b) axial stress amplitude variations of experimental alloy during in-phase tests at 0.5% axial strain amplitude and various shear strain amplitudes.

The effect of simultaneous axial deformation on the shape of shear hysteresis loop and the evolution of shear stress amplitude during proportional axial-torsional tests are shown in Figure 10. The proportional tests include pure torsional at 0.6%, and axial-torsional combining shear strain amplitude of 0.6% with different axial strain amplitudes of 0.3, 0.4 and 0.5%. According to Figure 10(a), while pure torsional hysteresis loop is symmetric, axial-torsional cyclic tests show asymmetric shear behaviour. With increasing axial strain amplitude, the asymmetry of shear hysteresis becomes more pronounced. We can even observe a sigmoidal-shape shear unloading reversal with axial strain amplitude of 0.5%. As was reported elsewhere [15], 0.5% corresponded to minimum axial strain amplitude to see de-twinning saturation during the tensile reversal of AM30 extrusion stabilized hysteresis loop. It is stated that the asymmetry of shear hysteresis loop is associated with the occurrence of twinning/de-twinning and the induced change in texture [7,8]. Upon reorienting matrix by twinning, basal slip is more favoured in the twinned portion of microstructure than the matrix. Hence, a higher volume fraction of twins under axial mode will result in easier shear strain accommodation under torsional mode. This is confirmed by the results presented in Figure 10(b).

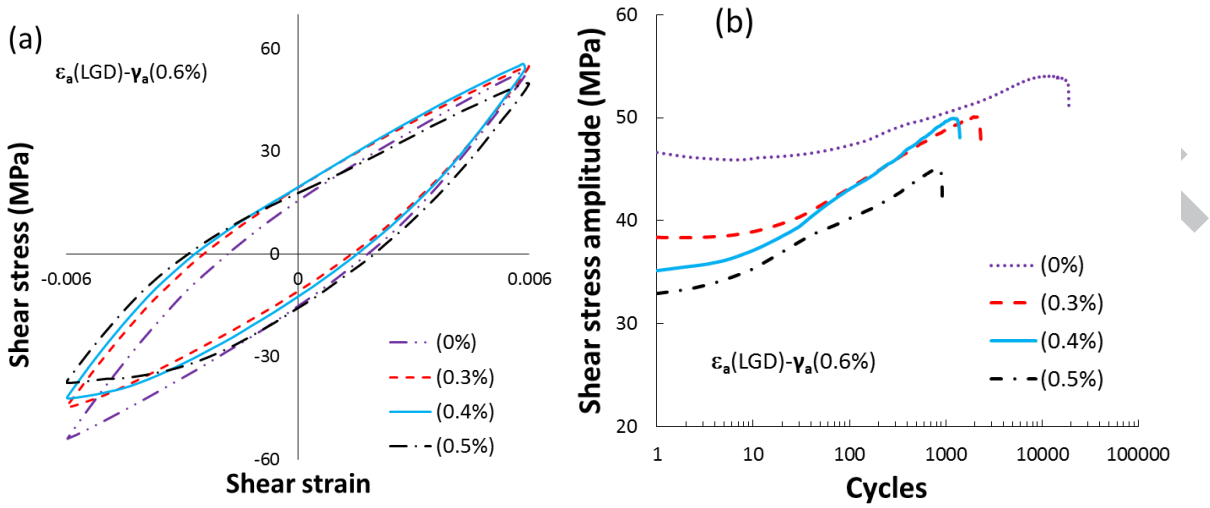

Figure 10. (a) Torsional stress-strain hysteresis loops and (b) shear stress amplitude variations of experimental alloy during in-phase tests at 0.6% shear strain amplitude and various axial strain amplitudes.

3.2.2. Phase angle effects

Figure 11 illustrates the effect of phase angle shift between axial and torsional sinusoidal waveforms on stabilized hysteresis loops at constant axial and shear strain amplitudes of 0.3% and 0.6%, respectively. No significant change in the overall shapes of hysteresis loops can be spotted. There is only a minor reduction of mean stress with increasing phase angle shift, which was also observed in AZ31B extrusion and attributed to the weaker resistance of microstructure to shear deformation in the presence of twins [8]. The volume fraction of twins at the negative tip of shear hysteresis loop is highest for in-phase and lowest for 90° out-of-phase strain path. (See **Error! Reference source not found.**).

The stabilized stress-strain hysteresis curves of AM30 extrusion subjected to axial and shear strain amplitudes of 0.5% and 0.6%, respectively, applied with different phase angle shifts of 0, 45 and 90° are shown in Figure 12. Contrary to the results presented in Figure 11, there is a noticeable change in the shapes of shear hysteresis loops with varying the phase angle shift, while axial hysteresis loops are remained unchanged. Similar observations in Mg alloy

extrusions were reported by other researchers [6,8,10]. The changes in shear hysteresis loops are ascribed to the twinning/de-twinning phenomena under axial deformation (see **Error! Reference source not found.**). It was mentioned earlier that axial strain amplitude of 0.5% during cyclic tension-compression test was found to be the threshold value for the predominance of twinning/de-twinning deformation mechanism at half-life. Therefore, it is concluded that axial hysteresis characteristics are not affected by the non-proportionality of multiaxial loading, whereas, depending on the magnitude of axial strain amplitude, phase angle shift can influence shear hysteresis loops.

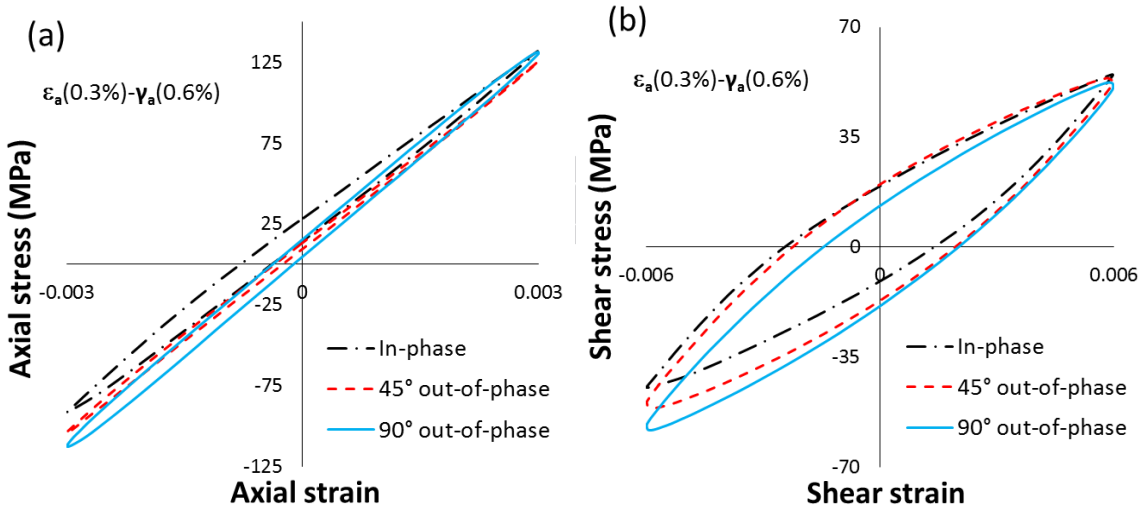

Figure 11. Axial and torsional hysteresis loops of AM30 extrusion during cyclic tests at ε_a= 0.3%, γ_a= 0.6% and different phase angle shifts.

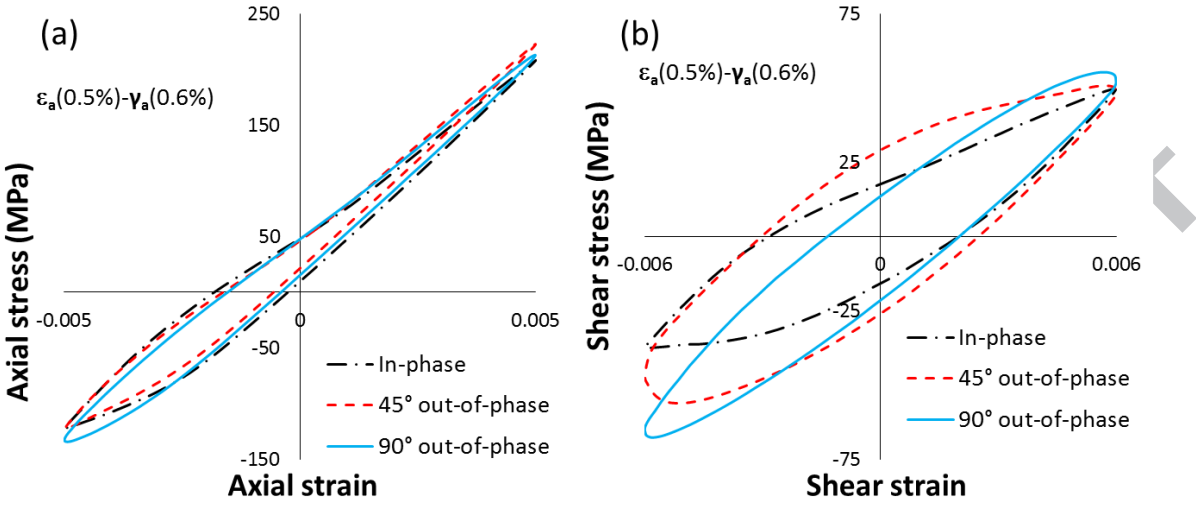

Figure 12. Axial and torsional hysteresis loops of AM30 extrusion during cyclic tests at ε_a= 0.5%, γ_a= 0.6% and different phase angle shifts.

Referring to the data in Table 1, fatigue lives obtained at $\varepsilon_a(0.3\%)$ and $\gamma_a(0.6\%)$ for the phase angle shifts of 0, 45 and 90° are 3210, 3141 and 3179 cycles, respectively. Furthermore, the fatigue lives at $\varepsilon_a(0.5\%)$ and $\gamma_a(0.6\%)$ for similar phase angle shifts are recorded to be 917, 650 and 829 cycles, respectively. It appears that phase angle shift has no significant effect on the fatigue lives obtained at $\varepsilon_a(0.3\%)$ and $\gamma_a(0.6\%)$, but affects the fatigue lives at $\varepsilon_a(0.5\%)$ and $\gamma_a(0.6\%)$. This may be elucidated by data in Figure 13, which shows that total strain energy densities measured at $\varepsilon_a(0.3\%)$ and $\gamma_a(0.6\%)$ with different phase angle shifts are comparable to each other (Figure 13(a)), while they are different for various phase angle shifts at $\varepsilon_a(0.5\%)$ and $\gamma_a(0.6\%)$ (Figure 13(b)).

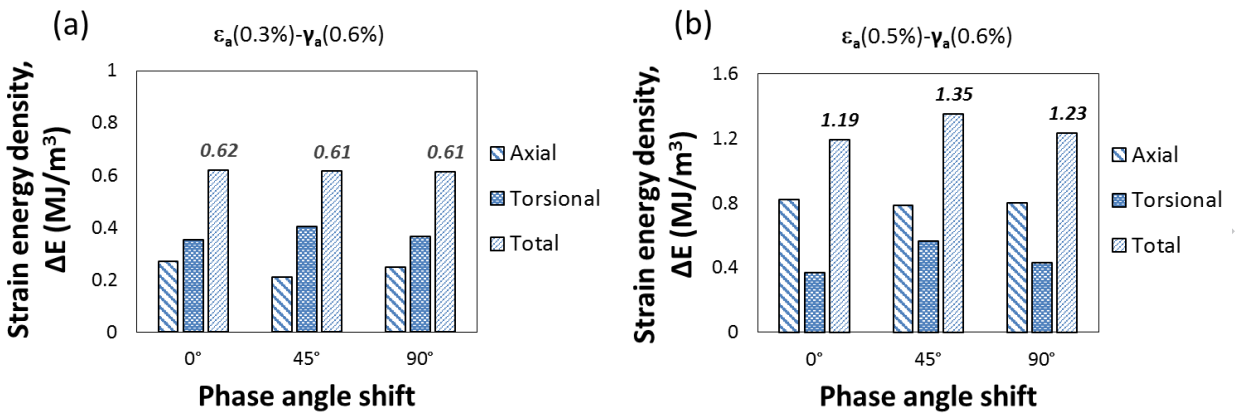

Figure 13. Measured axial and torsional strain energy densities for half-life hysteresis loops during cyclic tests at different phase angle shifts: (a) ε_a= 0.3%, γ_a= 0.6% and (b) ε_a= 0.5%, γ_a= 0.6%.

In order to explore the hardening behaviour of AM30 extrusion under combined axial-torsional loading, the variations of axial and shear stress amplitudes at $\varepsilon_a(0.5\%)$ and $\gamma_a(0.6\%)$ and different phase angle shifts are given in Figure 14. For comparison purposes, stress responses from pure axial (at ε_a= 0.5%) and pure torsional (at γ_a= 0.6%) cyclic tests are also included. It can be seen that with the increase of phase angle shift from 0 to 90°, higher stress amplitudes are exhibited in both axial and torsional modes. This additional non-proportional hardening is much more pronounced in the torsional mode (Figure 14(b)). Similar results were reported for AZ31B extrusion [10]. It is worth mentioning that the additional cyclic hardening is a general phenomenon, which happens due to the rotation of principal axes during out-of-phase loading [24]. For a grain with arbitrary orientation, the rotation of principal axes will result in the activation of various slip systems and twins along different orientations. Interaction between these activated mechanisms brings about the additional hardening.

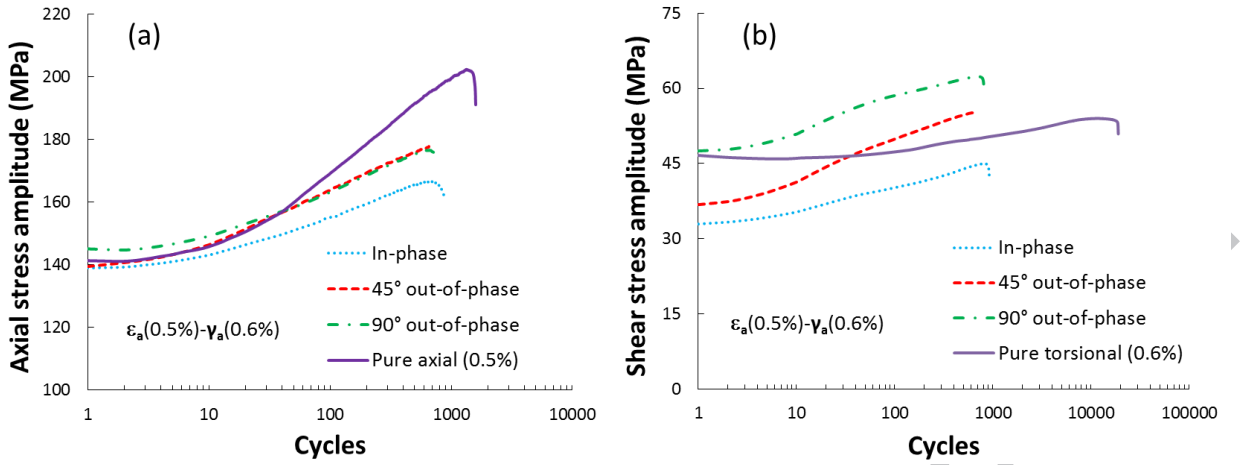

Figure 14. The variations of (a) axial and (b) shear stress amplitudes with cyclic straining at ε_a= 0.5%, γ_a= 0.6% with different phase angle shifts.

3.3. Fatigue modelling

Various fatigue damage parameters have been formulated to quantify damage caused to a material under cyclic loading. Critical plane approaches and energy-based models are being commonly applied to a variety of metals [11,13,25–27]. In critical plane approaches a critical plane of material is sought in a way that gives the maximum value of a predefined parameter. To this end, the parameters of interest from stabilized hysteresis loops are first transformed using stress-strain transformation rules (via Mohr's circle method). After pinpointing the critical plane, corresponding model parameters on that plane are extracted and used in a damage equation to find damage parameter. The damage parameter is, ultimately, coupled with a life equation to give life prediction. It is noteworthy that critical plane models are, theoretically, defined to predict early fatigue cracking orientation, in addition to final fatigue life. Nonetheless, this aspect of critical plane models is not being investigated here.

This section evaluates the fatigue life prediction capabilities of two common critical plane approaches, i.e., Fatemi-Socie and modified Smith-Watson-Topper, as well as Jahed-Varvani as an energy-based approach.

3.3.1. Fatemi-Socie (FS)

Fatemi-Socie model [24] was built on Brown and Miller's work [28] by replacing normal strain term with normal stress. The critical plane in this model is defined as the material plane with maximum shear strain value. Its fatigue damage parameter takes the following mathematical form:

$$FS\ Parameter = \gamma_{a,max}\left(1 + k\frac{\sigma_{n,max}}{\sigma_y}\right) \quad \text{Eq. 1}$$

where $\gamma_{a,max}$ is the maximum shear strain amplitude, $\sigma_{n,max}$ is the maximum normal stress on the maximum shear strain plane (critical plane), and k and σ_y are material constants. The constant k is found in a way that the curves of FS damage parameter versus number of reversals for pure axial (tension-compression) and pure torsional tests are brought together (k = 1.3 in this study). The constant σ_y is assumed equal to the monotonic yield strength of the material (200 MPa for AM30 extrusion). In Eq. (1), k/σ_y represents the sensitivity of a material to normal stress [29]. In Figure 15(a), the FS parameter is plotted as a function of number of reversals to failure under various loading conditions. Pure axial data were obtained from a previous article by the authors [15]. As is observed, calculated fatigue damage data using FS criterion are closely converged regardless of different testing circumstances. This confirms the capability of FS model for quantifying fatigue damage under combined axial-torsional cyclic deformation.

Based on FS model, the fatigue damage parameter may be correlated with fatigue life using shear strain-life properties of material. Hence, the following relationship is employed to estimate the fatigue life under different loading conditions:

$$FS\ Parameter = \frac{\tau_f'}{G}\left(2N_f\right)^{b_s} + \gamma_f'\left(2N_f\right)^{c_s} \quad \text{Eq. 2}$$

where G is the shear modulus (considered 15.1 GPa in this study), and N_f is the number of cycles to fatigue failure. The definitions of the shear strain-life parameters and their corresponding values for AM30 extrusion, calculated from Figure 15(b), are listed in Table 2. The symbols in Figure 15(b) correspond to experimental data obtained from half-life hysteresis loops of pure torsional tests and dashed lines are best power-law fits.

Table 2. Shear strain-life parameters used in FS model.

Shear fatigue strength coefficient, τ_f' (MPa)	283.818
Shear fatigue ductility coefficient, γ_f'	0.602
Shear fatigue strength exponent, b_s	-0.159
Shear fatigue ductility exponent, c_s	-0.531

The predicted fatigue lives by FS model are plotted against experimental lives under various loading conditions and is shown in Figure 15(c). Diagonal solid line represents perfect match and two parallel long-dashed and dash-dotted lines indicate factor of 2 and 1.5 bounds, respectively, between predicted and experimental lives. Based on the results, all predictions fall within factor of 2 boundaries, though the fatigue lives are mostly under-predicted, especially for pure axial tests in the low-cycle fatigue regime. In general, the results imply the capability of FS model to estimate the axial-torsional fatigue life of AM30 extrusion.

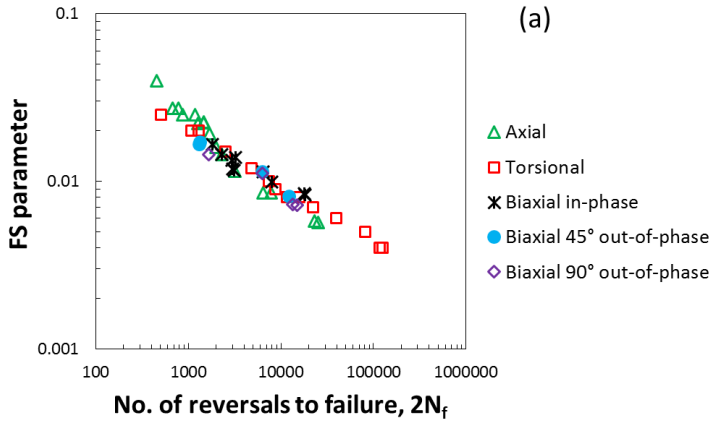

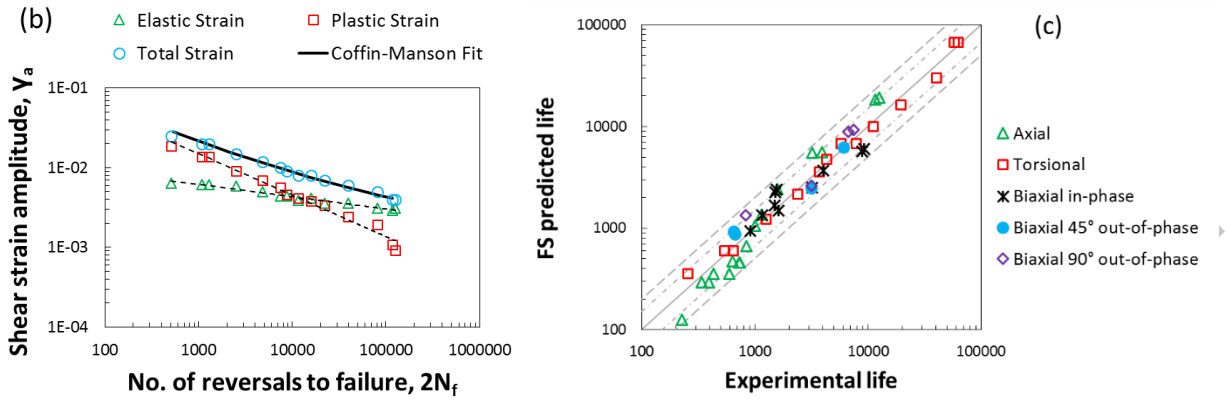

Figure 15. (a) Calculated FS parameters under various loading conditions; (b) Shear strain-life data used for extracting shear fatigue properties; (c) The correlation of FS-estimated life with experimental life.

3.3.2. Modified Smith-Watson-Topper (MSWT)

The SWT parameter has been used by Socie in the multiaxial loading analysis of materials that fail primarily under tensile cracking mode [29]. This critical plane model was shown to be incapable of correlating fatigue data under pure torsional loading of AZ31B extrusion [8,10]. Jiang and Sehitoglu [30] modified SWT parameter to take general cracking mode into account:

$$MSWT\ Parameter = 2b\,\Delta\varepsilon\,\sigma_{max} + \frac{1-b}{2}\Delta\tau\,\Delta\gamma \qquad \text{Eq. 3}$$

where $\Delta\varepsilon$, $\Delta\tau$ and $\Delta\gamma$ stand for the ranges of normal strain, shear stress and shear strain, respectively, and b is a material constant. The critical material plane in this model is defined as the plane with the maximum value of MSWT parameter. The variable b varies from 0 to 1. For b = 1, Eq. (3) gives the original SWT parameter. It is stated that for the values of b between 0.37 and 0.5, mixed cracking behaviour can be evaluated, while $b \leq 0.37$ and $b \geq 0.5$ enables the model to be used in shear and tensile cracking modes, respectively [6,8]. Figure 16(a) depicts the MSWT parameter calculated for different uniaxial and axial-torsional cyclic tests by assuming b = 0.3. The value of b implies that shear cracking mode is dominant in the experimental alloy.

According to Figure 16(b), the linear relationship between MSWT parameter and number of reversals to failure in a log-log scale can fairly be fitted employing a power-law equation:

$$MSWT\ Parameter = 67.136\left(2N_f\right)^{-0.473} \quad \text{Eq. 4}$$

Eq. (4) can be used, in conjunction with Eq. (3), to estimate fatigue life under various loading conditions. In Figure 16(c), the estimated fatigue lives are compared with the experimental ones. It can be deduced that the modified SWT model provides reasonably good fatigue life predictions for AM30 extrusion under pure uniaxial and combined axial-torsional loading. This model had been successfully applied to predict the multiaxial fatigue of AZ31B and AZ61A Mg alloys extrusions [6,8].

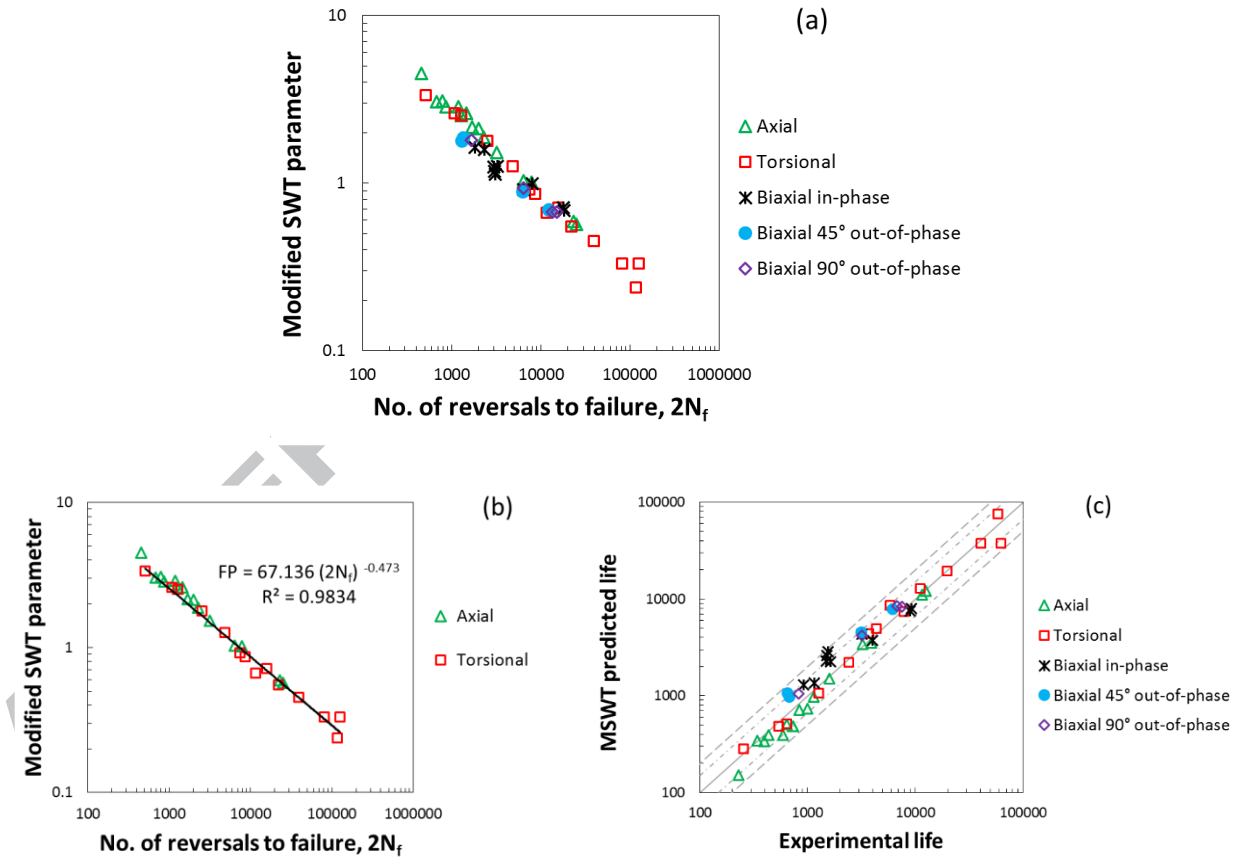

Figure 16. (a) Calculated modified SWT parameters under various loading conditions; (b) Power-law relationship between MSWT parameter and number of reversals to failure; (c) The correlation of MSWT-estimated life with experimental life.

3.3.3. Jahed-Varvani (JV)

Given the invariant nature of energy as a scalar quantity, energy-based approaches have the potential to be used for multiaxial fatigue life prediction of anisotropic materials such as AM30 Mg alloy extrusion. In current study, Jahed-Varvani's energy-based model [31] will be evaluated on the basis of its life prediction capabilities.

In the JV model, fatigue damage is expressed by total strain energy density, which consists of two different terms, i.e., plastic and positive elastic strain energy densities. The former term is calculated from area inside stabilized hysteresis loop at any strain amplitude:

$$\Delta E_A^p = \oint \sigma_{xx} d\varepsilon_{xx}^p$$

$$\Delta E_S^p = \oint \tau_{xy} d\gamma_{xy}^p \qquad \text{Eq. 5}$$

where ΔE_A^p and ΔE_S^p are plastic axial and torsional strain energy densities, respectively. Positive elastic energy can be determined by the following equations:

$$\Delta E_{e,A}^+ = \frac{{\sigma_{max}}^2}{2E}$$

$$\Delta E_{e,S}^+ = \frac{{\tau_{max}}^2}{2G} \qquad \text{Eq. 6}$$

where σ_{max} and τ_{max} are, respectively, axial and shear stresses at the positive tip of the hysteresis loops, and *E* and *G* are, respectively, the average tensile and average shear moduli of unloading reversals. By introducing positive elastic strain energy density, mean stress effects are also taken into account in this model [32,33]. The axial and shear strain energy densities are, then, related to fatigue life in terms of number of reversals to failure through an equation similar to Coffin-Manson relationship [31,34]:

$$\Delta E_A = E_e'(2N_A)^B + E_f'(2N_A)^C$$

$$\Delta E_S = W_e'(2N_S)^{B_s} + W_f'(2N_S)^{C_s} \qquad \text{Eq. 7}$$

where ΔE_A and $2N_A$ are total axial strain energy density and axial fatigue life in reversals, respectively, and ΔE_S and $2N_S$ are their shear counterparts. The remaining symbols in Eq. (7) denote energy-based fatigue parameters, which are defined in Table 3.

In order to find the energy-based fatigue parameters, pure axial and pure torsional cyclic tests of AM30 extrusion are utilized to construct the plots of positive elastic/plastic axial/shear energy densities versus fatigue life in log-log scale, as shown in Figure 17(a) and (b). From these plots, the energy-based fatigue parameters are determined and tabulated in Table 3.

Table 3. Energy-based fatigue parameters used in JV model.

Axial fatigue strength coefficient, E'_e (MJ/m^3)	9.107
Axial fatigue toughness coefficient, E'_f (MJ/m^3)	20350.770
Axial fatigue strength exponent, B	-0.340
Axial fatigue toughness exponent, C	-1.378
Shear fatigue strength coefficient, W'_e (MJ/m^3)	2.762
Shear fatigue toughness coefficient, W'_f (MJ/m^3)	318.753
Shear fatigue strength exponent, B_s	-0.325
Shear fatigue toughness exponent, C_s	-0.683

To assess the fatigue life of the experimental alloy under various proportional and non-proportional axial-torsional loading conditions, first axial and shear strain energy densities from stabilized hysteresis loops should be computed. Next, these values together with energy-based fatigue parameters are used in Eq. (7) to give two fatigue lives; N_A and N_S. These lives correspond to upper and lower bounds for each loading scenario. The actual fatigue life falls at some value between N_A and N_S [31]. In this study, the following equation is observed to result in best life estimations by combining two fatigue life limits:

$$N_f = \frac{\Delta E_A}{\Delta E_T} N_A + \frac{1}{2}\frac{\Delta E_S}{\Delta E_T} N_S \qquad \text{Eq. 8}$$

where N_f is the final estimated life, and ΔE_T is total strain energy density (sum of axial and shear components). The comparison between JV predicted life and the experimental life is illustrated in Figure 17(c). The long-dashed lines represent the factor of 2 limits and dash-dotted lines show the factor of 1.5 boundaries. It is clear that the JV model provides very good predictions within the life factor range of ±1.5.

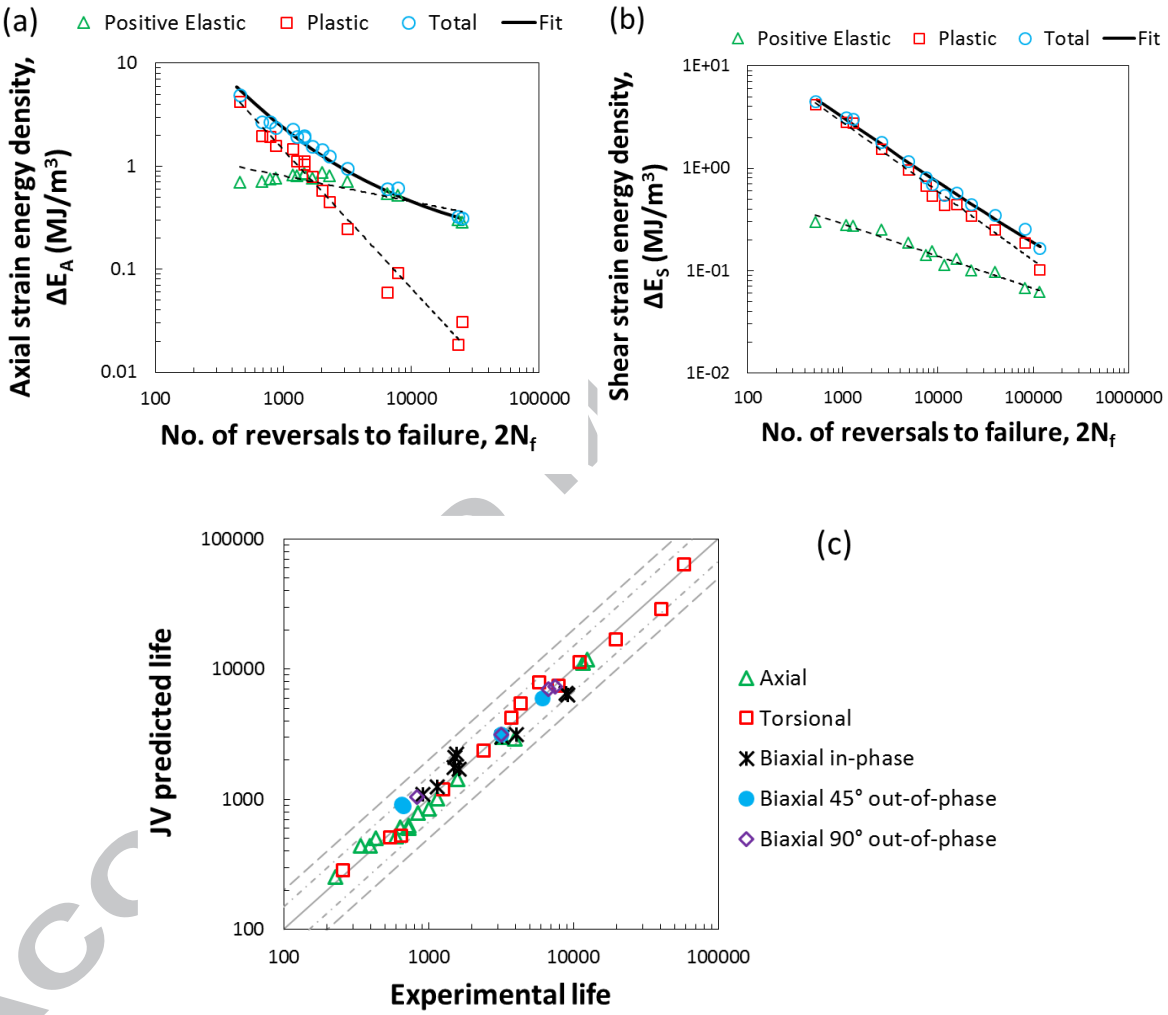

Figure 17. (a) Axial and (b) shear strain energy density-life data used for extracting JV model parameters; (c) The correlation of JV-estimated life with experimental life.

4. Conclusions

Pure torsional and combined axial-torsional cyclic tests under fully-reversed strain-controlled conditions have been performed on AM30 Mg alloy extrusion. The following main points can be restated from the discussed results:

1) AM30 extrusion exhibits symmetric hysteresis loops upon pure torsional cyclic loading. Slip is, accordingly, considered predominant deformation mechanism, although twinning is proved to happen at very large shear strain amplitudes.
2) AM30 extrusion displays better low-cycle shear fatigue properties than AZ31B and AZ61A extrusions, during strain-controlled cyclic tests.
3) During proportional biaxial cyclic tests, twinning/de-twinning occurrence in axial mode renders the shear response asymmetric. On the other hand, shear deformation is found to only affect the slip-dominated portion of axial hysteresis loop.
4) Axial hysteresis characteristics are not affected by the non-proportionality of multiaxial loading, whereas, depending on the magnitude of axial strain amplitude, phase angle shift can alter shear hysteresis loops.
5) Additional non-proportional hardening is seen for both axial and torsional modes, during combined biaxial deformation of AM30 extrusion.
6) Both critical plane approaches, namely, Fatemi-Socie and Modified Smith-Watson-Topper, as well as Jahed-Varvani energy-based model can suitably predict fatigue life of AM30 Mg alloy extrusion under multiaxial loading conditions.

Acknowledgments

This study was partially funded by the Natural Sciences and Engineering Research Council (NSERC) under Automotive Partnership of Canada (APC) program (Grant no. APCPJ

459269-13). The financial support of the Government of Ontario through Ontario Trillium Scholarship (OTS) program is also acknowledged.

References

[1] Eliezer D, Aghion E, Froes FH. Magnesium science, technology and applications. Advanced Performance Materials 1998;5:201–12. doi:10.1023/A:1008682415141.

[2] Bettles C, Gibson M. Current wrought magnesium alloys: Strengths and weaknesses. JOM 2005;57:46–9. doi:10.1007/s11837-005-0095-0.

[3] Friedrich H, Schumann S. Research for a "new age of magnesium" in the automotive industry. Journal of Materials Processing Technology 2001;117:276–81. doi:10.1016/S0924-0136(01)00780-4.

[4] Kulekci MK. Magnesium and its alloys applications in automotive industry. International Journal of Advanced Manufacturing Technology 2008;39:851–65. doi:10.1007/s00170-007-1279-2.

[5] Bentachfine S, Pluvinage G, Toth LS, Azari Z. Biaxial low cycle fatigue under non-proportional loading of a magnesium-lithium alloy. Engineering Fracture Mechanics 1996;54:513–22. doi:10.1016/0013-7944(95)00223-5.

[6] Yu Q, Zhang J, Jiang Y, Li Q. Multiaxial fatigue of extruded AZ61A magnesium alloy. International Journal of Fatigue 2011;33:437–47. doi:10.1016/j.ijfatigue.2010.09.020.

[7] Zhang J, Yu Q, Jiang Y, Li Q. An experimental study of cyclic deformation of extruded AZ61A magnesium alloy. International Journal of Plasticity 2011;27:768–87. doi:10.1016/j.ijplas.2010.09.004.

[8] Xiong Y, Yu Q, Jiang Y. Multiaxial fatigue of extruded AZ31B magnesium alloy. Materials Science and Engineering A 2012;546:119–28. doi:10.1016/j.msea.2012.03.039.

[9] Albinmousa J, Jahed H. Multiaxial effects on LCF behaviour and fatigue failure of AZ31B magnesium extrusion. International Journal of Fatigue 2014;67:103–16. doi:10.1016/j.ijfatigue.2014.01.025.

[10] Albinmousa J, Jahed H, Lambert S. Cyclic behaviour of wrought magnesium alloy under multiaxial load. International Journal of Fatigue 2011;33:1127–39. doi:10.1016/j.ijfatigue.2011.01.009.

[11] Jahed H, Albinmousa J. Multiaxial behaviour of wrought magnesium alloys - A review

and suitability of energy-based fatigue life model. Theoretical and Applied Fracture Mechanics 2014;73:97–108. doi:10.1016/j.tafmec.2014.08.004.

[12] Albinmousa J, Jahed H, Lambert S. Cyclic axial and cyclic torsional behaviour of extruded AZ31B magnesium alloy. International Journal of Fatigue 2011;33:1403–16. doi:10.1016/j.ijfatigue.2011.04.012.

[13] Castro F, Jiang Y. Fatigue life and early cracking predictions of extruded AZ31B magnesium alloy using critical plane approaches. International Journal of Fatigue 2016;88:236–46. doi:10.1016/j.ijfatigue.2016.04.002.

[14] Li H, Kang G, Liu Y, Jiang H. Non-proportionally multiaxial cyclic deformation of AZ31 magnesium alloy: Experimental observations. Materials Science and Engineering: A 2016;671:70–81. doi:10.1016/j.msea.2016.06.043.

[15] Roostaei AA, Jahed H. Role of loading direction on cyclic behaviour characteristics of AM30 extrusion and its fatigue damage modelling. Materials Science and Engineering: A 2016;670:26–40. doi:10.1016/j.msea.2016.05.116.

[16] Luo AA, Sachdev AK. Development of a New Wrought Magnesium-Aluminum-Manganese Alloy AM30. Metallurgical and Materials Transactions A 2007;38A:1184–92. doi:10.1007/s11661-007-9129-2.

[17] Albinmousa J, Pascu A, Jahed H, Horstemeyer MF, Luo A, Chen D, et al. Monotonic and Fatigue Behavior of Magnesium Extrusion Alloy AM30: An International Benchmark Test in the "Magnesium Front End Research and Development Project." SAE Technical Papers, vol. 2010-01–04, 2010, p. 1–12. doi:10.4271/2010-01-0407.

[18] Begum S, Chen DL, Xu S, Luo AA. Strain-Controlled Low-Cycle Fatigue Properties of a Newly Developed Extruded Magnesium Alloy. Metallurgical and Materials Transactions A 2008;39:3014–26. doi:10.1007/s11661-008-9722-z.

[19] Lou XY, Li M, Boger RK, Agnew SR, Wagoner RH. Hardening evolution of AZ31B Mg sheet. International Journal of Plasticity 2007;23:44–86. doi:10.1016/j.ijplas.2006.03.005.

[20] Sonsino CM. Influence of material's ductility and local deformation mode on multiaxial fatigue response. International Journal of Fatigue 2011;33:930–47. doi:10.1016/j.ijfatigue.2011.01.010.

[21] Wu L, Jain A, Brown DW, Stoica GM, Agnew SR, Clausen B, et al. Twinning-detwinning behavior during the strain-controlled low-cycle fatigue testing of a wrought magnesium

alloy, ZK60A. Acta Materialia 2008;56:688–95. doi:10.1016/j.actamat.2007.10.030.

[22] Brown DW, Agnew SR, Bourke MAM, Holden TM, Vogel SC, Tomé CN. Internal strain and texture evolution during deformation twinning in magnesium. Materials Science and Engineering A 2005;399:1–12. doi:10.1016/j.msea.2005.02.016.

[23] Wu W, Liaw PK, An K. Unraveling cyclic deformation mechanisms of a rolled magnesium alloy using in situ neutron diffraction. Acta Materialia 2015;85:343–53. doi:10.1016/j.actamat.2014.11.030.

[24] Fatemi A, Socie DF. A Critical Plane Approach To Multiaxial Fatigue Damage Including Out-of-Phase Loading. Fatigue & Fracture of Engineering Materials and Structures 1988;11:149–65. doi:10.1111/j.1460-2695.1988.tb01169.x.

[25] Jiang Y, Hertel O, Vormwald M. An experimental evaluation of three critical plane multiaxial fatigue criteria. International Journal of Fatigue 2007;29:1490–502. doi:10.1016/j.ijfatigue.2006.10.028.

[26] You BR, Lee SB. A critical review on multiaxial faigue assessments of metals. International Journal of Fatigue 1996;18:235–44.

[27] Liu KC. A Method Based on Virtual Strain-Energy Parameters for Multiaxial Fatigue Life Prediction. In: McDowell DL, Ellis J, editors. Advances in Multiaxial Fatigue, ASTM STP 1191, 100 Barr Harbor Drive, PO Box C700, West Conshohocken, PA 19428-2959: ASTM International; 1993, p. 67–84. doi:10.1520/STP24796S.

[28] Brown MW, Miller KJ. A theory for fatigue failure under multiaxial stress–strain conditions. Proceedings of the Institution of Mechanical Engineers 1847-1982 (Vols 1-196) 1973;187:745–55. doi:10.1243/PIME_PROC_1973_187_161_02.

[29] Socie DF, Marquis GB. Multiaxial Fatigue. Warrendale, Pa: SAE International; 2000.

[30] Jiang Y, Sehitoglu H. Fatigue and stress analysis of rolling contact. College of Engineering, University of Illinois at Urbana-Champaign 1992;Rep no.161.

[31] Jahed H, Varvani-Farahani A. Upper and lower fatigue life limits model using energy-based fatigue properties. International Journal of Fatigue 2006;28:467–73. doi:10.1016/j.ijfatigue.2005.07.039.

[32] Ellyin F, Golos K, Xia Z. In-Phase and Out-of-Phase Multiaxial Fatigue. Journal of Engineering Materials and Technology 1991;113:112–8.

[33] Golos K, Ellyin F. A Total Strain Energy Density Theory for Cumulative Fatigue

Damage. Journal of Pressure Vessel Technology 1988;110:36–41. doi:10.1115/1.3226012.

[34] Jahed H, Varvani-Farahani A, Noban M, Khalaji I. An energy-based fatigue life assessment model for various metallic materials under proportional and non-proportional loading conditions. International Journal of Fatigue 2007;29:647–55. doi:10.1016/j.ijfatigue.2006.07.017.

- AM30 extrusion shows better low-cycle shear fatigue properties than AZ31B, AZ61A.
- Non-proportionality of biaxial loading does not affect axial hysteresis loops.
- Phase angle shift effects on shear hysteresis loops depend on axial strain level.
- Additional non-proportional hardening is seen for both axial and torsional modes.
- Critical plane and energy models give reliable multiaxial fatigue life estimations.